

Article

Open Access



# Ultra-long $\text{Zn}_3\text{V}_2\text{O}_7(\text{OH})_2 \cdot 2\text{H}_2\text{O}$ nanowires grown on carbon cloth as cathode material for aqueous zinc-ion batteries

Yu Cui<sup>1,#</sup>, Yi Ding<sup>2,#</sup>, Lingfan Guo<sup>2</sup>, Chunli Guo<sup>2,\*</sup>, Yanzen Liu<sup>3,\*</sup>, Yulin Bai<sup>4</sup>, Gang Li<sup>1</sup>, Kaiying Wang<sup>1</sup>

<sup>1</sup>Institute of Energy Innovation, College of Materials Science and Engineering, Taiyuan University of Technology, Taiyuan 030024, Shanxi, China.

<sup>2</sup>College of Materials Science and Engineering, Taiyuan University of Technology, Taiyuan 030024, Shanxi, China.

<sup>3</sup>State Key Laboratory of Coal Conversion, Institute of Coal Chemistry, Chinese Academy of Science, Taiyuan 030001, Shanxi, China.

<sup>4</sup>College of Aeronautics and Astronautics, Taiyuan University of Technology, Taiyuan 030024, Shanxi, China.

#Authors contributed equally.

\*Correspondence to: Prof. Chunli Guo, College of Materials Science and Engineering, Taiyuan University of Technology, No. 79 West Street Yingze, Taiyuan 030024, Shanxi, China. E-mail: guochunli@tyut.edu.cn; Dr. Yanzen Liu, State Key Laboratory of Coal Conversion, Institute of Coal Chemistry, Chinese Academy of Science, 27 South Taoyuan Road, Taiyuan 030001, Shanxi, China. E-mail: liuyz@sxicc.ac.cn

**How to cite this article:** Cui Y, Ding Y, Guo L, Guo C, Liu Y, Bai Y, Li G, Wang K. Ultra-long  $\text{Zn}_3\text{V}_2\text{O}_7(\text{OH})_2 \cdot 2\text{H}_2\text{O}$  nanowires grown on carbon cloth as cathode material for aqueous zinc-ion batteries. *Energy Mater* 2023;3:300023. <https://dx.doi.org/10.20517/energymater.2022.90>

**Received:** 12 Dec 2022 **First Decision:** 16 Feb 2023 **Revised:** 10 Apr 2023 **Accepted:** 27 Apr 2023 **Published:** 12 May 2023

**Academic Editors:** Jiazhao Wang, Wei Tang **Copy Editor:** Fangling Lan **Production Editor:** Fangling Lan

## Abstract

Enhancing the performance of the cathode materials is one of the key issues for aqueous zinc-ion batteries (AZIBs). Layered vanadium-based compounds are considered to be a candidate cathode material for AZIBs owing to their advantages of variable crystal structures and high-theoretical capacity. Nevertheless, the inherent low conductivity of V-based compounds leads to their sluggish kinetics and serious capacity degradation of AZIBs. Here, we proposed a strategy that combined morphology regulation with self-supporting electrodes to build an efficient electron/ion transport network and prepared  $\text{Zn}_3(\text{OH})_2\text{V}_2\text{O}_7 \cdot 2\text{H}_2\text{O}$  (ZVO) nanowires (ZVNW) on carbon cloth (CC) by a hydrothermal method. As expected, the ZVNW-CC electrode showed excellent electrochemical performances of a high specific capacity of  $361.8 \text{ mAh g}^{-1}$  ( $50 \text{ mA g}^{-1}$ ), high-rate capability ( $145.9 \text{ mAh g}^{-1}$  discharge capacity at  $1,000 \text{ mA g}^{-1}$ ), and long cycling life (96.7% capacity retention after 1,010 cycles at  $1,000 \text{ mA g}^{-1}$ ). The  $\text{Zn}^{2+}/\text{H}_2\text{O}$  co-intercalation mechanism for ZVNW-CC electrodes was demonstrated by *ex-situ* XPS and *ex-situ* TGA.



© The Author(s) 2023. **Open Access** This article is licensed under a Creative Commons Attribution 4.0 International License (<https://creativecommons.org/licenses/by/4.0/>), which permits unrestricted use, sharing, adaptation, distribution and reproduction in any medium or format, for any purpose, even commercially, as long as you give appropriate credit to the original author(s) and the source, provide a link to the Creative Commons license, and indicate if changes were made.



**Keywords:** Aqueous zinc-ion batteries, cathode material,  $\text{Zn}_3(\text{OH})_2\text{V}_2\text{O}_7 \cdot 2\text{H}_2\text{O}$ , carbon cloth, zinc storage mechanism

## INTRODUCTION

Nowadays, there are two determining factors in the development of lithium-ion batteries (LIBs): safety and cost price. The rechargeable aqueous Zn-ion batteries (AZIBs) are considered as a preferred solution due to their high level of safety, low cost, and environmental friendliness<sup>[1-4]</sup>. However, the wide application of AZIBs has been seriously hampered by the lack of high-performance cathode materials. Layered vanadium-based compounds with an open framework structure can facilitate the fast Zn-ion intercalation/deintercalation and enhance the specific capacities. Besides, the multiple oxidation states of vanadium can further contribute to increasing the specific capacity<sup>[5-9]</sup>.

$\text{Zn}_3(\text{OH})_2\text{V}_2\text{O}_7 \cdot 2\text{H}_2\text{O}$  (ZVO) materials became a powerful competitor among all vanadium-based compounds. This was because the structural water located between the V-O layers, which was attached by hydrogen bonds to hydroxyl groups, enlarged the interlayer spacing, leading to high capacity and high-rate capability<sup>[10,11]</sup>. While they were commonly used as cathode electrodes in LIBs, only a few studies reported their usage in AZIBs. For example, Li *et al.* developed hexagonal ZVO nanoplates by a hydrothermal route and applied them as a cathode material for AZIBs<sup>[12]</sup>. The ZVO electrode displayed a discharge capacity of 117.69 mAh g<sup>-1</sup> at a current density of 50 mA g<sup>-1</sup>. Xia *et al.* reported ultra-long ZVO nanowires (ZVNW) by a microwave method<sup>[13]</sup>. The ZVNW were utilized as a cathode for AZIBs and showed a high capacity of 213 mAh g<sup>-1</sup> at 50 mA g<sup>-1</sup> due to the short Zn<sup>2+</sup> diffusion channel<sup>[13]</sup>. However, their inherent low conductivity caused sluggish charge transfer kinetics. Recently, the N-doping carbon as an effective conductive support was doped into ZVNW, which exhibited a large capacity of 295 mAh g<sup>-1</sup> at 0.1 A g<sup>-1</sup><sup>[14]</sup>. However, multiple interfaces formed among the active materials, additives (such as ancillary binders) and collectors could impede the mass transfer, leading to the unsatisfied performances.

To address these issues, the carbon cloth (CC) with high conductivity, light weight, and excellent structural stability has been used as the growth template to ensure the orientation of active materials and as collectors<sup>[15-18]</sup> to fasten the electron transport due to the strong attachment between the active materials and CC. In this study, we first prepared the ultra-long ZVO nanowires on CC (ZVNW-CC) through a hydrothermal route. ZVNW-CC was directly utilized as a cathode for AZIBs and exhibited a high specific capacity of 361.8 mAh g<sup>-1</sup> (at 50 A g<sup>-1</sup>). ZVNW-CC electrodes displayed higher rate performance and more favorable cycle retention than pristine ZVNW, indicating that the construction of an efficient electron/ion transport path of ZVNW-CC cathode for AZIBs was beneficial to the improvement of electrochemical performance.

## EXPERIMENT

### Preparation of $\text{Zn}_3(\text{OH})_2\text{V}_2\text{O}_7 \cdot 2\text{H}_2\text{O}$ nanowires grown on carbon cloth

All the chemicals used in this study were analytical grade without any further purification. They were purchased from Sinopharm Group Chemical Reagent Co. CC (3 × 3 cm) was pretreated by immersing it in a mixture solution of 20% nitric acid and sulfuric acid (v/v 1:1) for 12 h. Then  $\text{NH}_4\text{VO}_3$  (2 mmol) and  $\text{ZnSO}_4 \cdot 6\text{H}_2\text{O}$  (3 mmol) were dissolved into 60 mL deionized water at 80 °C to form a clear, light yellow solution. Later, 7 mL  $\text{H}_2\text{O}$  was added to the solution. Subsequently, they were transferred to a 100 mL polytetrafluoroethylene-lined container along with the pretreated CC. The mixture was heated at 180 °C for 14 h and cooled naturally. Finally, the prepared CC was moved out and washed with deionized water and ethanol several times, then dried at 60 °C for 12 h to obtain the sample (ZVNW-CC). A synthesis diagram

of the ZVNW-CC synthesis process was shown in [Supplementary Figure 1](#). The preparation process of ZVNW was the same as the above-mentioned steps, except that CC was not used.

### Sample characterization

For crystallographic analysis, the as-obtained samples were characterized by the powder X-ray diffraction (XRD, Cu K $\alpha$  radiation,  $\lambda = 1.5418 \text{ \AA}$ ). Surface elemental oxidation states were identified by X-ray photoelectron spectroscopy (XPS, Thermo Scientific Escalab 250Xi) using Al K $\alpha$  as the X-ray source. The spectrometer was calibrated by the C 1s peak with a binding energy of 284.6 eV. The surface structure was obtained using field-emission scanning electron microscopy (FE-SEM, S-4700 Hitachi). The lattice fringes were analyzed using field-emission transmission electron microscopy (FE-TEM, Philips Tecnai F20 at 200 kV). The weight changes of the sample were examined by a thermal gravimetric analyzer (Netzsch STA 449E3) at 800 °C with a heating rate of 5 °C min<sup>-1</sup> in N<sub>2</sub>.

### Electrode preparation and electrochemical performance

A ZVNW-CC electrode disk (diameter: 12 mm) was used directly as a cathode, zinc foil (diameter: 16 mm) as an anode, and a Whatman CF/F separator was placed between the electrodes. The electrodes were assembled using a 2016-type coin cell and tested in 3 M Zn(CF<sub>3</sub>SO<sub>3</sub>)<sub>2</sub> solution. The active material loading was approximately 3 mg cm<sup>-2</sup>. For comparison, a ZVNW cathode was fabricated by casting a slurry mixture of 70 wt% active material, 20 wt% acetylene black, and 10 wt% polyvinylidene fluoride (PVDF) binder in N-methylpyrrolidone (NMP) on Ti foil. The mixture was then dried at 60 °C for 12 h under vacuum. Cyclic voltammetry (CV) was performed over a potential range of 0.2 to 1.6 V (vs. Zn<sup>2+</sup>/Zn) at 0.1 mV s<sup>-1</sup>. Galvanostatic charge/discharge (GCD) cycling was conducted at various current rates. CV tests were performed on a CHI 600E electrochemical station. All the tests were performed at room temperature.

## RESULTS AND DISCUSSION

### Structural and phase analysis

The as-obtained sample was characterized by XRD. [Figure 1](#) shows that the diffraction peaks at 12.3°, 16.9°, 20.9°, 24.7°, 30.1°, 32.1°, 34.2°, 36.5°, 38.9°, 42.7°, 51.6°, and 62.6° corresponded to (001), (100), (011), (002), (102), (111), (200), (201), (112), (202), (203), and (204) planes of hexagonal Zn<sub>3</sub>(OH)<sub>2</sub>V<sub>2</sub>O<sub>7</sub>·2H<sub>2</sub>O (JCPDS NO. 87-0417), respectively. In addition, the diffraction peak intensity of (001) is much higher than that of (102), suggesting the [001] direction (c-axis) crystallographic preferred orientations of ZVNW. The inset image in [Figure 1](#) shows the crystal structure of Zn<sub>3</sub>V<sub>2</sub>O<sub>7</sub>(OH)<sub>2</sub>·2H<sub>2</sub>O, which consists of a Zn-O layer formed by edge-sharing [ZnO<sub>6</sub>] octahedra and a V-O layer. The Zn-O layers were separated by V-O-V pillars formed by corner-sharing [VO<sub>4</sub>] tetrahedra along the c-axis. Water molecules were randomly filled in the large cavities<sup>[19]</sup>. [Supplementary Figure 2](#) indicates the XRD pattern of ZVNW-CC. The carbon peaks at 26° were clearly observed because the content of ZVNW was lower than that of CC.

To further characterize the valence state and composition of ZVNW-CC, the XPS techniques were performed. [Figure 2A](#) shows the overall XPS spectrum of ZVNW-CC, illustrating that it is composed of Zn, V, O, and C elements. [Figure 2B](#) shows the high-resolution XPS spectrum of Zn 2p. The peaks centered at binding energies of 1045.0 and 1021.9 eV were attributed to Zn 2p<sub>1/2</sub> and Zn 2p<sub>3/2</sub>, respectively. And their binding energy difference was about 23.1 eV, proving the existence of Zn<sup>2+</sup><sup>[13,20]</sup>. [Figure 2C](#) is a high-resolution V 2p XPS spectrum of ZVNW-CC. The binding energies of the fitted peaks corresponding to V 2p<sub>1/2</sub> and V 2p<sub>3/2</sub> were 524.7 eV and 517.4 eV, respectively, indicating the existence of V<sup>5+</sup><sup>[20]</sup>. The XPS spectrum of O 1s was performed in [Figure 2D](#), and the fitted peaks at 530.1, 530.8, and 532.8 eV corresponded to O<sup>2-</sup>, O-H bond, and H<sub>2</sub>O molecule, respectively.

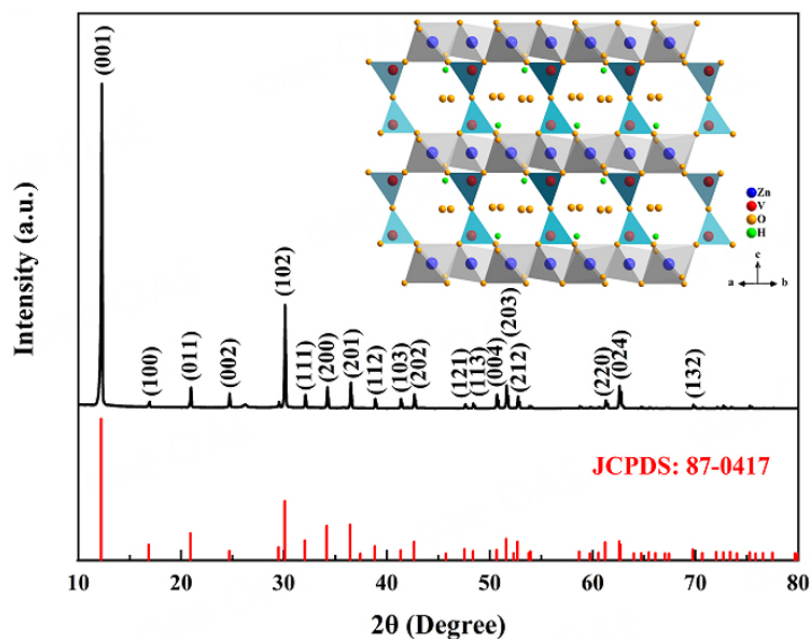


Figure 1. XRD patterns of ZVNW.

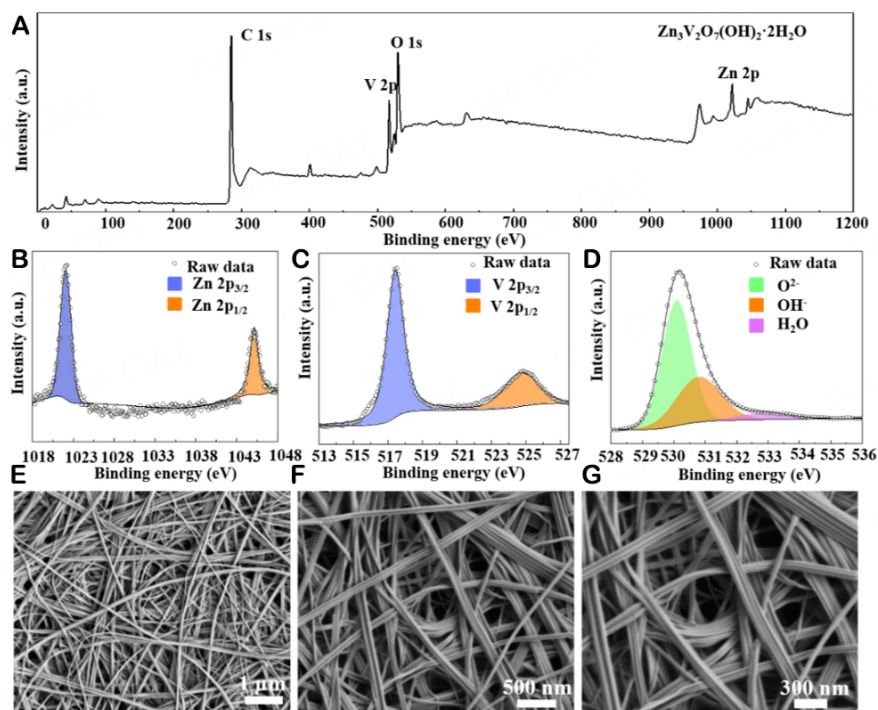


Figure 2. XPS spectra: (A) overall spectrum. (B) Zn 2p. (C) V 2p. (D) O 1s. SEM images at different magnifications (E-G) of ZVNW-CC.

### Morphology and microstructure analysis

The morphologies of ZVNW-CC and ZVNW were characterized by SEM in [Figure 2E-G](#) and [supplementary Figure 3](#). The ZVNW with tens of microns grown on CC in parallel can be clearly observed in [Figure 2E](#). The length of each nanowire can reach the micron level. This structure was beneficial for

increasing the contact area between ZVNW and CC, which enhanced the structural stability of the ZVNW-CC electrode. And 1D nanostructure can shorten the diffusion pathway of  $\text{Zn}^{2+}$  during the charging and discharging process, promoting the electrochemical performance of the ZVNW-CC electrode. SEM images in [Figure 2F](#) and [G](#) show a higher-resolution view of the sample. ZVNW, ranging in size from 20-200 nm, was stacked and interlaced grown on CC, forming a multi-void network structure.

The microstructure of ZVNW, peeled from CC through prolonged sonication, was further characterized by TEM. [Figure 3A](#) shows a TEM image of a single ZVO nanowire. The surface of the ZVNW was rough, which increased the contact area between the electrode and electrolyte. [Figure 3B](#) is its HRTEM image. The inter-planar distances of 2.01 and 2.31 Å were attributed to (210) and (112) planes of ZVO, respectively. [Figure 3C](#) shows the fast Fourier transform electron diffraction (FFT-ED) pattern of the HRTEM image, which suggests the single-crystal feature. [Figure 3D](#) shows the EDS analysis of a single ZVO nanowire. It was further confirmed that the ZVNW were composed of Zn, V, and O elements, which were uniformly distributed in the ZVNW.

### Electrochemical performances

The electrochemical properties of ZVNW and ZVNW-CC electrodes were evaluated by CV and GCD. [Figure 4A](#) shows the CV curves of these two electrodes at  $0.1 \text{ mV s}^{-1}$ . The surrounding CV curve area of the ZVNW-CC electrode was much larger than that of the ZVNW electrode, indicating that the ZVNW-CC electrode exhibited higher specific capacity. [Figure 4B](#) presents the first three cycles of the CV plot for the ZVNW-CC electrode at a scan rate of  $0.1 \text{ mV s}^{-1}$  in the voltage range of 0.2-1.6 V (*vs.*  $\text{Zn}/\text{Zn}^{2+}$ ). Three pairs of redox peaks were observed at 0.56/0.76, 0.85/1.07, and 1.35/1.46 V, which were attributed to the three-step reaction of  $\text{Zn}^{2+}$  insertion and extraction into the ZVO lattice structure<sup>[21]</sup>. Among the reduction reactions at 0.56, 0.85, and 1.35 V showed that the vanadium element in ZVNW-CC was gradually reduced from +5 valence to  $+a$  ( $a < 5$ ), and the oxidation reactions at 0.76, 1.07, and 1.46 V corresponded to the gradual oxidation of  $\text{V}^{a+}$  to  $\text{V}^{5+}$ . The cyclic scanning process of the first three loops almost overlapped, indicating that the storage process of  $\text{Zn}^{2+}$  was highly reversible. GCD tests were conducted between 0.2 and 1.6 V (*vs.*  $\text{Zn}/\text{Zn}^{2+}$ ). [Figure 4C](#) and [D](#) indicates the GCD profiles of ZVNW-CC and ZVNW electrodes for the first five and 50th cycles at  $50 \text{ mA g}^{-1}$ . In the discharge curve, there were two distinctive potential plateaus within the range of 0.69-1.00 and 0.45-0.69 V, which corresponded to the two main oxidation peaks of CV. Similarly, another two potential plateaus in the charge curve within 0.88-1.15 and 0.6-0.88 V corresponded to the reduction peaks. The related charge-discharge curve of ZVNW-CC electrodes at  $50 \text{ mA g}^{-1}$  exhibited a smaller overpotential ( $\Delta V(Q/2)$ ) than that of the ZVNW electrode (0.26 *vs.* 0.34 V, [Figure 4C](#) and [D](#)). In sharp contrast, the specific capacity of the ZVNW-CC electrode was larger than that of the ZVNW electrode, benefitting from the synergistic effects of morphology regulation and a self-supporting electrode.

The rate performances are presented in [Figure 5A](#), where the current density increases from 50 to  $1,000 \text{ mA g}^{-1}$  and then returns to  $50 \text{ mA g}^{-1}$ . The ZVNW-CC cathode displayed specific capacities of 361.8, 328.2, 292.8, 251.1, and  $207.6 \text{ mAh g}^{-1}$  at 50, 100, 200, 500, and  $800 \text{ mA g}^{-1}$ , respectively. Even at  $1,000 \text{ mA g}^{-1}$ , the ZVNW-CC cathode can still deliver a reversible capacity of  $145.9 \text{ mAh g}^{-1}$ . And returning to  $50 \text{ mA g}^{-1}$ , the specific capacity of  $346.9 \text{ mAh g}^{-1}$  and the capacity recovery of 95.8% can still be obtained. However, the capacities of the ZVNW electrode were evidently lower than those of ZVNW-CC at every corresponding current density. This indicated that the structural stability and electrochemical reversibility of the ZVNW-CC cathode were much superior to those of the ZVNW electrode. In order to assess the commercial potential of the ZVNW-CC electrode, long-cycle performance testing was necessary. The cycling performances of the ZVNW and ZVNW-CC electrodes were examined at current densities of 200, 500, and  $1,000 \text{ mA g}^{-1}$ , respectively, and were shown in [Figure 5B-D](#). The discharge capacity of the ZVNW-

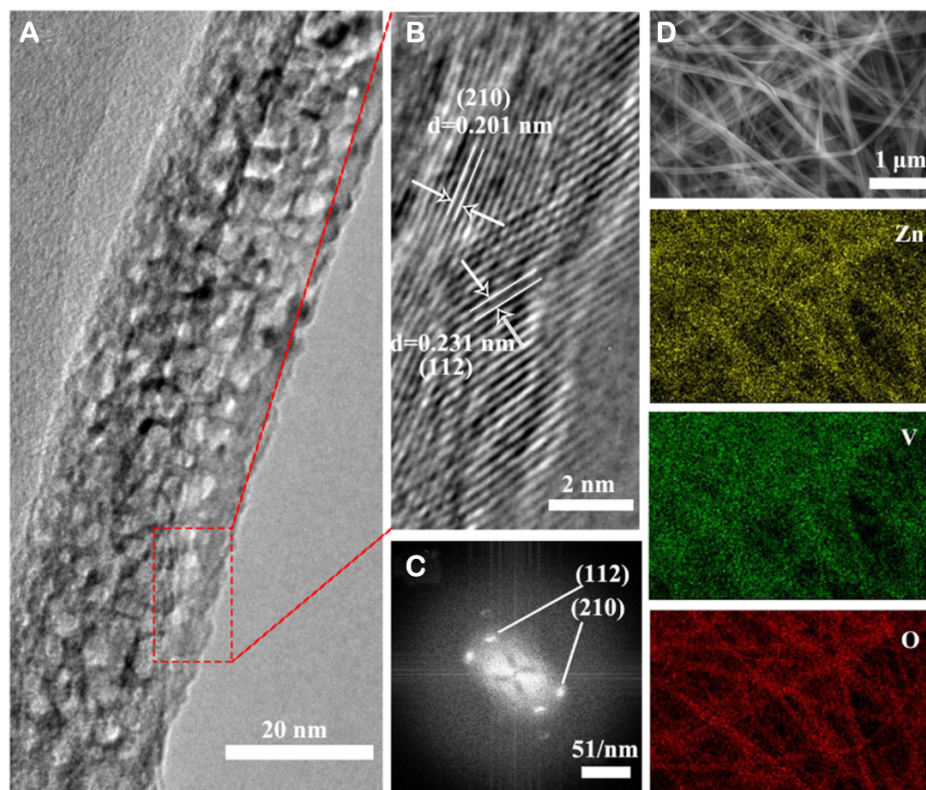


**Figure 3.** (A) TEM image. (B) HRTEM image. (C) FFT-ED pattern (D) EDS mapping of ZVNW peeled from CC through prolonged sonication.

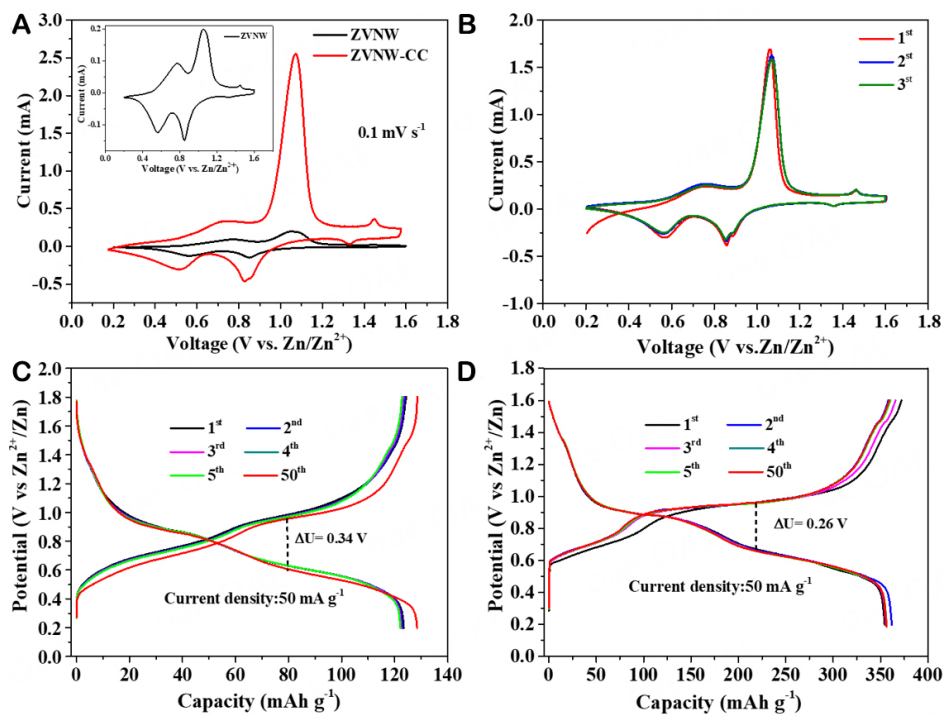


**Figure 4.** (A) CV curves of ZVNW and ZVNW-CC electrodes. (B) CV curves of ZVNW-CC electrode in the first three cycles at  $0.1 \text{ mV s}^{-1}$ . GCD curves of ZVNW (C) and ZVNW-CC (D) electrodes at different cycles.

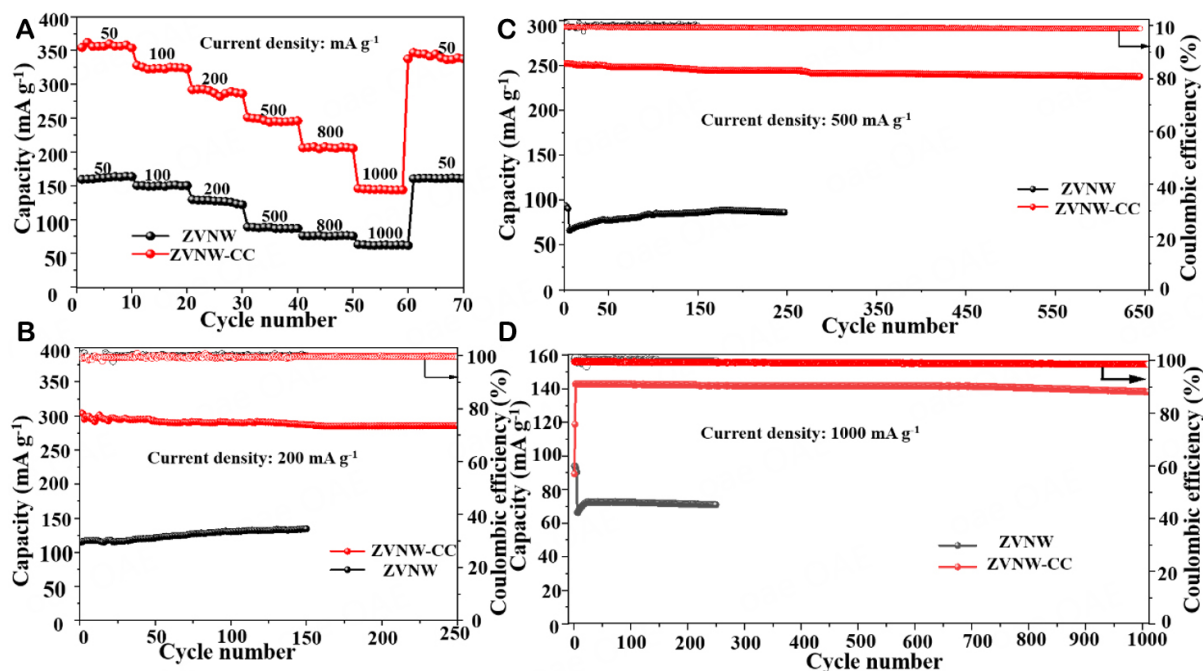


**Figure 5.** (A) The rate capability of ZVNW-CC and ZVNW electrodes. The cycling stability of ZVNW-CC and ZVNW electrodes at (B) 200, (C) 500, and (D) 1,000  $\text{mA g}^{-1}$ .

CC cathode reached up to  $285.9 \text{ mAh g}^{-1}$  at  $200 \text{ mA g}^{-1}$  and the capacity retention rate was 93.7% after 250 cycles. The ZVNW-CC electrode released a specific capacity of  $237.7 \text{ mAh g}^{-1}$  with a capacity retention rate of 94.2% after 645 cycles at  $500 \text{ mA g}^{-1}$ . Even at  $1,000 \text{ mA g}^{-1}$ , a specific capacity of  $138.2 \text{ mAh g}^{-1}$  with 96.7% capacity retention after 1,010 cycles and nearly 100% Coulombic efficiency were maintained, indicating its excellent cycle stability at the high current densities. However, both the cycling performance and specific capacity of the ZVNW electrode were unsatisfactory. Therefore, the integrated ZVNW-CC electrode was conductive, which improved the electrochemical performance of the half cell. Compared with other similar reported electrodes (as shown in Table 1), the ZVNW-CC electrode in this study exhibited high specific capacity and stable long-cycle performance.

### Electrochemical kinetic properties and zinc storage mechanism

The Zn-ion storage behavior of the ZVNW-CC electrode was further studied by CV. Figure 6A presents the CV curves of the ZVNW-CC cathode measured at different scan rates. The CV curves retained the same shape with the increase of scan rates from  $0.1$  to  $0.5 \text{ mV s}^{-1}$ , indicating good reversibility of the ZVNW-CC cathode. A power law relationship with the sweep rate:  $i = av^b$ , or  $\log i = b \log v + \log a$  (peak current:  $i$ , scan speed:  $v$ , and adjustable parameters:  $a$  and  $b$ ), was used to calculate the contributions of capacitive and diffusion-controlled processes in AZIBs. Among them, if the value of  $b$  was close to 1.0, then the electrochemical process was controlled by the capacitive effect; when  $b = 0.5$ , the process was controlled by ion diffusion; if  $0.5 < b < 1.0$ , both ion diffusion and capacitance effects were involved. Figure 6B shows the plot of  $\log(i)$  versus  $\log(v)$  for calculation of the  $b$  value. The  $b$  values of peak (1) and peak (2) in Figure 6A were 0.7 and 1.0, respectively, indicating a contribution process dominated by capacity control. To further clarify the details of electrochemical behavior, GITT measurement was implemented to study the  $\text{Zn}^{2+}$  diffusion coefficients ( $D_{\text{Zn}^{2+}}$ ) of the ZVNW-CC electrode.  $D_{\text{Zn}^{2+}}$  can be estimated according to Supplementary Figure 4 and Eq. 1 in the supporting information. Each cycle consisted of charging to  $1.6 \text{ V}$  at a rate of  $50 \text{ mA g}^{-1}$  for 20 min, relaxing for 2 h, and discharging to  $0.2 \text{ V}$  at the same rate. Figure 6C shows

**Table 1. Comparison of the specific capacity and cycling performance of ZVNW-CC electrode with other reported cathodes in AZIBs**

Samples	Specific capacity (mAh g <sup>-1</sup> )	Capacity retention	Refs
ZVO-CC	361.8 (0.05 A g <sup>-1</sup> )	80% (650 cycles)	This work
Zn <sub>3</sub> V <sub>2</sub> O <sub>7</sub> (OH) <sub>2</sub> ·2H <sub>2</sub> O	213 (0.05 A g <sup>-1</sup> )	68% (300 cycles)	[13]
V <sub>2</sub> O <sub>5</sub>	319 (0.02 A g <sup>-1</sup> )	81% (500 cycles)	[22]
LiV <sub>3</sub> O <sub>8</sub>	256 (0.016 A g <sup>-1</sup> )	75% (65 cycles)	[23]
KV <sub>3</sub> O <sub>8</sub>	249 (0.025 A g <sup>-1</sup> )	82.8% (500 cycles)	[24]
Zn <sub>2</sub> V <sub>2</sub> O <sub>7</sub>	203 (0.3 A g <sup>-1</sup> )	85% (1,000 cycles)	[25]
K <sub>2</sub> V <sub>6</sub> O <sub>16</sub> ·2.7H <sub>2</sub> O	329.6 (0.2 A g <sup>-1</sup> )	82% (500 cycles)	[26]
VS <sub>2</sub>	190.3 (0.05 A g <sup>-1</sup> )	98% (200 cycles)	[27]
Na <sub>3</sub> V <sub>2</sub> (PO <sub>4</sub> ) <sub>3</sub>	97 (0.05 A g <sup>-1</sup> )	74% (100 cycles)	[28]
VS <sub>4</sub> @rGO	180 (1 A g <sup>-1</sup> )	93.3% (165 cycles)	[29]

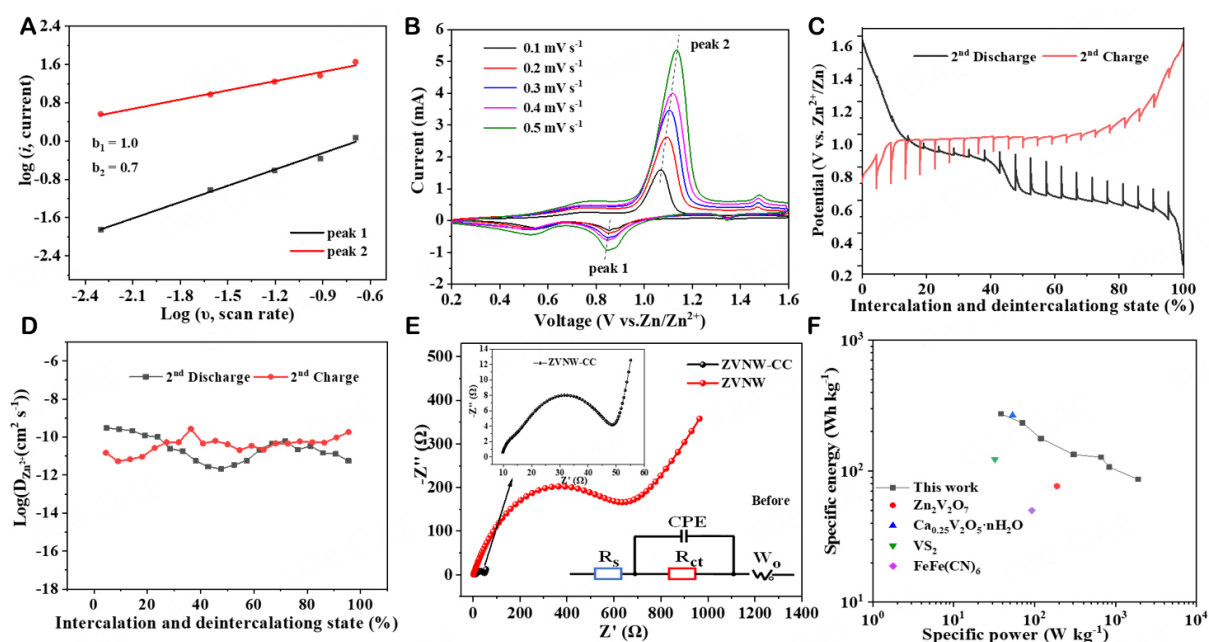


**Figure 6.** (A) CV curves of the ZVNW-CC electrode at different scan rates. (B)  $b$  value of the redox peak in the CV curve. (C) GITT curves during discharge and charge. (D) Corresponding  $Zn^{2+}$  diffusion coefficient during the 2nd cycle of charge-discharge. (E) Nyquist plots of ZVNW-CC and ZVNW electrodes before cycling in the frequency range of 0.01 Hz to 100 kHz. (F) The Ragone plot comparison of Zn/ZVNW-CC battery with other cathode materials for AZIBs.

the GITT data at the second cycle taken from the charge-discharge curve.  $D_{Zn^{2+}}$  was calculated between  $10^{-9}$  and  $10^{-11}$  cm<sup>2</sup> s<sup>-1</sup> (as shown in Figure 6D), which is superior to those of some reported V-based cathode materials in AZIBs<sup>[30-33]</sup>.

The electrochemical impedance spectroscopy measurement was performed to evaluate the charge transfer resistance of the ZVNW-CC and ZVNW electrodes before and after cycling (as shown in Figure 6E and Supplementary Figure 5). Figure 6E displays the Nyquist plots of these two cathodes before cycling and their equivalent circuit models. The diameter of the semi-circle in the Nyquist plots of ZVNW-CC, associated with the contact resistance and charge transfer processes ( $R_{ct}$ ), was far less than that of the ZVNW electrode. It meant that the  $R_{ct}$  value of the ZVNW-CC electrode was significantly decreased without any additives<sup>[34,35]</sup>.  $R_{ct}$  values of ZVNW-CC and ZVNW electrodes before (after) cycling were 41.4 (34.3) and

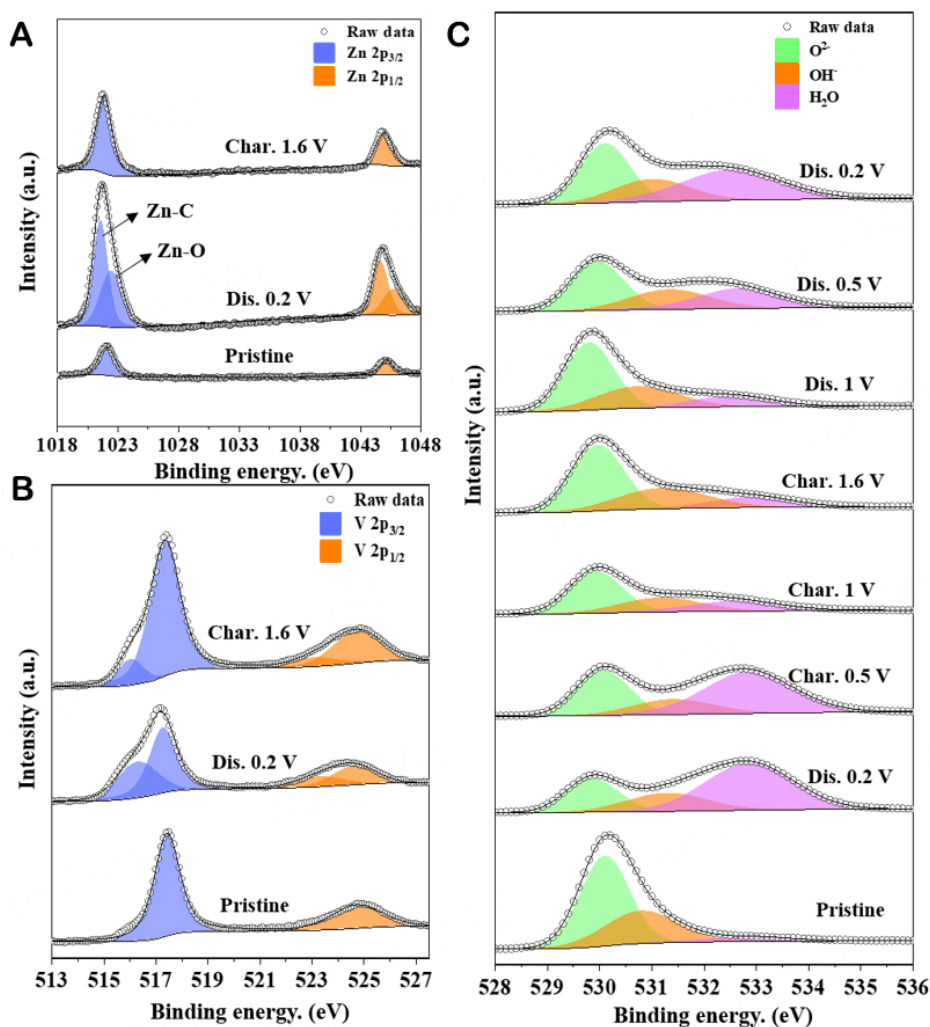
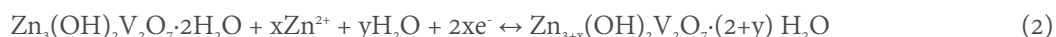


**Figure 7.** Ex-situ high-resolution XPS spectra of ZVNW-CC electrodes at different charge-discharge states: (A) V 2p. (B) Zn 2p. (C) O1s.

603.5 (109.1)  $\Omega$ , respectively, indicating the improved conductivity of the self-supporting electrode. The above results further proved that both the 1D ZVNW-CC cathode and self-supporting electrode together fastened the  $\text{Zn}^{2+}$  immigration, resulting in high capacity and high cycle stability. Moreover, the energy density and power density of the ZVNW-CC electrode were calculated to be 273.5  $\text{Wh kg}^{-1}$  and 1,888  $\text{W kg}^{-1}$ , respectively. Compared with the reported AZIBs containing similar cathodes such as  $\text{Ca}_{0.25}\text{V}_2\text{O}_5 \cdot n\text{H}_2\text{O}$  [21],  $\text{Zn}_2\text{V}_2\text{O}_7$  [25],  $\text{VS}_2$  [27], and  $\text{FeFe}(\text{CN})_6$  [36], the ZVNW-CC electrode provided higher energy densities in a wide range of power densities in Ragone plots (as shown in Figure 6F).

*Ex situ* XPS analyses were used to analyze the valence-state change of the ZVNW-CC electrode and further revealed the possible  $\text{Zn}^{2+}$  storage mechanism during the charge and discharge processes. Figure 7A shows the Zn 2p spectra of the fully charged and fully discharged states of the ZVNW-CC electrode. In the fully discharged state, Zn  $2p_{3/2}$  peaks at 1,022.48 and 1,021.58 eV or Zn  $2p_{1/2}$  peaks at 1,045.76 and 1,044.67 eV were due to the formation of Zn-O and Zn-C bonds [37]. However, in the fully charged state, only the XPS peak of the Zn-O bond remained and the Zn-C peak disappeared, which suggested that  $\text{Zn}^{2+}$  of Zn-C was more easily de-intercalated and led to an increase in capacitance. Moreover, with the interaction of  $\text{Zn}^{2+}$ , the

$V^{5+}$  of V-O-V pillars underwent a reduction reaction to  $V^{\alpha+}$  ( $\alpha < 5$ ), as shown in Figure 7B. In addition, the high-resolution XPS spectra of O 1s (as shown in Figure 7C) revealed its evolution at the pristine, fully discharged/charged states, respectively. Notably, the relative intensity of the crystal  $H_2O$  peak in the fully discharged ZVNW-CC decreased significantly during charging, further confirming the co-intercalation mechanism of  $Zn^{2+}$  and  $H_2O$ . Subsequently, thermogravimetric tests (nitrogen atmosphere) were also performed on ZVNW-CC electrodes under different charge and discharge conditions, as shown in Supplementary Figure 6. It was consistent with the XPS results. Based on the above analysis and discussion, the electrochemical reactions that occurred inside the Zn/ZVNW-CC batteries can be described by the following equations:



## CONCLUSIONS

We have designed the “self-supporting” electrode by 1D ZVNW grown on CC as the cathode material in AZIBs. Integrating the excellent electronic conductivity of CC, 1D ZVO nanowire with layered framework structure in ZVNW-CC can facilitate  $Zn^{2+}$  diffusion and fasten the electron transport, improving the electrochemical reaction kinetics of the electrode. Consequently, the ZVNW-CC electrode showed excellent electrochemical performances of a specific capacity of  $361.8 \text{ mAh g}^{-1}$  ( $50 \text{ mA g}^{-1}$ ), a high-rate capability ( $145.9 \text{ mAh g}^{-1}$  discharge capacity at  $1,000 \text{ mA g}^{-1}$ ), and long cycling life (96.7% capacity retention after 1,010 cycles at  $1,000 \text{ mA g}^{-1}$ ). The  $Zn^{2+}/H_2O$  co-intercalation mechanism in ZVNW-CC electrodes was demonstrated by *ex-situ* XPS and *ex-situ* TGA. The novel strategy proposed in this study may provide guidance for exploiting high-performance energy storage systems.

## DECLARATIONS

### Authors' contribution

Preparing the manuscript draft: Cui Y

Carried out the synthesis and characterization, performed the electrochemical measurements and characterizations: Cui Y, Ding Y, Guo L

Conceived the concept and directed the research, Writing-review & editing: Guo C, Liu Y

Provided the research advice: Liu Y, Bai Y

Supervision, Resources: Li G, Wang K

### Availability of data and materials

Not applicable.

### Financial support and sponsorship

This study was supported by the National Nature Science Foundation of China (Grant nos. U1910210, U1810204, 22278291, and 22105142) and Research Foundation for the Returned Overseas in Shanxi Province (2020-048).

### Conflicts of interest

All authors declared that there are no conflicts of interest.

### Ethical approval and consent to participate

Not applicable.

## Consent for publication

Not applicable.

## Copyright

© The Author(s) 2023.

## REFERENCES

1. Xu C, Li B, Du H, Kang F. Energetic zinc ion chemistry: the rechargeable zinc ion battery. *Angew Chem Int Ed* 2012;51:933-5. DOI PubMed
2. Hwang B, Cheong JY, Matteini P, Yun TG. Highly efficient phthalocyanine based aqueous Zn-ion flexible-batteries. *Mater Lett* 2022;306:130954. DOI
3. Yang W, Yang Y, Yang H, Zhou H. Regulating water activity for rechargeable zinc-ion batteries: progress and perspective. *ACS Energy Lett* 2022;7:2515-30. DOI
4. Zhang Y, Huang R, Wang X, et al. Facile large-scale preparation of vanadium pentoxide-polyppyrrrole composite for aqueous zinc-ion batteries. *J Alloys Compd* 2022;907:164434. DOI
5. Chen R, Luo R, Huang Y, Wu F, Li L. Advanced high energy density secondary batteries with multi-electron reaction materials. *Adv Sci* 2016;3:1600051. DOI PubMed PMC
6. Tang H, Peng Z, Wu L, et al. Vanadium-based cathode materials for rechargeable multivalent batteries: challenges and opportunities. *Electrochem Energy Rev* 2018;1:169-99. DOI
7. Wan F, Niu Z. Design strategies for vanadium-based aqueous zinc-ion batteries. *Angew Chem Int Ed* 2019;58:16358-67. DOI PubMed
8. Liu N, Li B, He Z, Dai L, Wang H, Wang L. Recent advances and perspectives on vanadium- and manganese-based cathode materials for aqueous zinc ion batteries. *J Energy Chem* 2021;59:134-59. DOI
9. Yuan Z, Chen X, Liu X, Feng C. Synthesis of  $Zn_3V_2O_7(OH)_2 \cdot 2H_2O$  microspheres as novel anode material for lithium-ion battery application. *Ionics* 2020;26:1703-10. DOI
10. Bulbul B, Beyaz S, Akyol M, Ekcibil A. Simple manufacturing and metal type-dependent properties of  $M_3(OH)_2V_2O_7 \cdot nH_2O$  (M; Co, Ni, Cu, Zn) nanostructures. *Nanochem Res* 2022;2:154-67. DOI
11. Du Y, Liu X, Wang X, et al. Freestanding strontium vanadate/carbon nanotube films for long-life aqueous zinc-ion batteries. *Rare Metals* 2021;41:415-24. DOI
12. Li L, Jia T, Pei X, et al. A study on the properties of hexagonal  $Zn_3(OH)_2V_2O_7 \cdot 2H_2O$  as cathode material for zinc-ion battery. *Ionics* 2022;28:283-93. DOI
13. Xia C, Guo J, Lei Y, Liang H, Zhao C, Alshareef HN. Rechargeable aqueous zinc-ion battery based on porous framework zinc pyrovanadate intercalation cathode. *Adv Mater* 2018;30:1705580. DOI
14. Wang F, Wang Q, Dong S, Wang S. An aqueous zinc pyrovanadate nanowire cathode doped by nitrogen-doped carbon from PANI calcination for capacity and stability enhancement. *Ionics* 2022;28:295-305. DOI
15. Zhao S, Guo J, Jiang F, Su Q, Du G. Porous  $CoFe_2O_4$  nanowire arrays on carbon cloth as binder-free anodes for flexible lithium-ion batteries. *Mater Res Bull* 2016;79:22-8. DOI
16. Storan D, Ahad SA, Forde R, et al. Silicon nanowire growth on carbon cloth for flexible Li-ion battery anodes. *Mater Today Energy* 2022;27:101030. DOI
17. Corpuz RD, Juan-Corpuz LM, Nguyen MT, et al. Binder-free  $\alpha$ - $MnO_2$  nanowires on carbon cloth as cathode material for zinc-ion batteries. *Int J Mol Sci* 2020;21:3113. DOI PubMed PMC
18. De Juan-corpuz LM, Corpuz RD, Somwangthanaroj A, et al. Binder-free centimeter-long  $V_2O_5$  nanofibers on carbon cloth as cathode material for zinc-ion batteries. *Energies* 2020;13:31. DOI
19. Jia X, Liu C, Neale ZG, Yang J, Cao G. Active materials for aqueous zinc ion batteries: synthesis, crystal structure, morphology, and electrochemistry. *Chem Rev* 2020;120:7795-866. DOI
20. Biesinger MC, Lau LW, Gerson AR, Smart RS. Resolving surface chemical states in XPS analysis of first row transition metals, oxides and hydroxides: Sc, Ti, V, Cu and Zn. *Appl Surf Sci* 2010;257:887-98. DOI
21. Xia C, Guo J, Li P, Zhang X, Alshareef HN. Highly stable aqueous zinc-ion storage using a layered calcium vanadium oxide bronze cathode. *Angew Chem Int Ed* 2018;57:3943-8. DOI
22. Chen X, Wang L, Li H, Cheng F, Chen J. Porous  $V_2O_5$  nanofibers as cathode materials for rechargeable aqueous zinc-ion batteries. *J Energy Chem* 2019;38:20-5. DOI
23. Alfaruqi MH, Mathew V, Song J, et al. Electrochemical zinc intercalation in lithium vanadium oxide: a high-capacity zinc-ion battery cathode. *Chem Mater* 2017;29:1684-94. DOI
24. Kim HJ, Jo JH, Choi JU, Voronina N, Myung S.  $KV_3O_8$  with a large interlayer as a viable cathode material for zinc-ion batteries. *J Power Sources* 2020;478:229072. DOI
25. Sambandam B, Soundharrajan V, Kim S, et al. Aqueous rechargeable Zn-ion batteries: an imperishable and high-energy  $Zn_2V_2O_7$  nanowire cathode through intercalation regulation. *J Mater Chem A* 2018;6:3850-6. DOI

26. Sambandam B, Soundharajan V, Kim S, et al.  $K_2V_6O_{16} \cdot 2.7H_2O$  nanorod cathode: an advanced intercalation system for high energy aqueous rechargeable Zn-ion batteries. *J Mater Chem A* 2018;6:15530-9. DOI
27. He P, Yan M, Zhang G, et al. Layered  $VS_2$  nanosheet-based aqueous Zn ion battery cathode. *Adv Energy Mater* 2017;7:1601920. DOI
28. Li G, Yang Z, Jiang Y, et al. Towards polyvalent ion batteries: a zinc-ion battery based on NASICON structured  $Na_3V_2(PO_4)_3$ . *Nano Energy* 2016;25:211-7. DOI
29. Qin H, Yang Z, Chen L, et al. A high-rate aqueous rechargeable zinc ion battery based on the  $VS_4@rGO$  nanocomposite. *J Mater Chem A* 2018;6:23757-65. DOI
30. Tang B, Fang G, Zhou J, et al. Potassium vanadates with stable structure and fast ion diffusion channel as cathode for rechargeable aqueous zinc-ion batteries. *Nano Energy* 2018;51:579-87. DOI
31. Guo X, Fang G, Zhang W, et al. Mechanistic insights of  $Zn^{2+}$  storage in sodium vanadates. *Adv Energy Mater* 2018;8:1801819. DOI
32. He P, Quan Y, Xu X, et al. High-performance aqueous zinc-ion battery based on layered  $H_2V_3O_8$  nanowire cathode. *Small* 2017;13:1702551. DOI
33. Zhang N, Jia M, Dong Y, et al. Hydrated layered vanadium oxide as a highly reversible cathode for rechargeable aqueous zinc batteries. *Adv Funct Mater* 2019;29:1807331. DOI
34. Tataru R, Karayaylali P, Yu Y, et al. The effect of electrode-electrolyte interface on the electrochemical impedance spectra for positive electrode in Li-ion battery. *J Electrochem Soc* 2019;166:A5090-8. DOI
35. Dong L, Yang W, Yang W, et al. High-power and ultralong-life aqueous zinc-ion hybrid capacitors based on pseudocapacitive charge storage. *Nanomicro Lett* 2019;11:94. DOI PubMed PMC
36. Liu Z, Bertram P, Endres F. Bio-degradable zinc-ion battery based on a prussian blue analogue cathode and a bio-ionic liquid-based electrolyte. *J Solid State Electrochem* 2017;21:2021-7. DOI
37. Zhang F, Sun X, Du M, et al. Weaker interactions in  $Zn^{2+}$  and organic ion-pre-intercalated vanadium oxide toward highly reversible zinc-ion batteries. *Energy Environ Mater* 2021;4:620-30. DOI